

# Murine neural stem cells model Hunter disease *in vitro*: glial cell-mediated neurodegeneration as a possible mechanism involved

E Fusar Poli<sup>1,2,7</sup>, C Zalfa<sup>1,7</sup>, F D'Avanzo<sup>3</sup>, R Tomanin<sup>3</sup>, L Carlessi<sup>2</sup>, M Bossi<sup>4</sup>, L Rota Nodari<sup>1</sup>, E Binda<sup>1</sup>, P Marmiroli<sup>4</sup>, M Scarpa<sup>3,5</sup>, D Delia<sup>2</sup>, AL Vescovi<sup>1,5,6</sup> and L De Filippis<sup>\*,1</sup>

Mucopolysaccharidosis type II (MPSII or Hunter Syndrome) is a lysosomal storage disorder caused by the deficit of iduronate 2-sulfatase (IDS) activity and characterized by progressive systemic and neurological impairment. As the early mechanisms leading to neuronal degeneration remain elusive, we chose to examine the properties of neural stem cells (NSCs) isolated from an animal model of the disease in order to evaluate whether their neurogenic potential could be used to recapitulate the early phases of neurogenesis in the brain of Hunter disease patients. Experiments here reported show that NSCs derived from the subventricular zone (SVZ) of early symptomatic IDS-knockout (IDS-ko) mouse retained self-renewal capacity *in vitro*, but differentiated earlier than wild-type (wt) cells, displaying an evident lysosomal aggregation in oligodendroglial and astroglial cells. Consistently, the SVZ of IDS-ko mice appeared similar to the wt SVZ, whereas the cortex and striatum presented a disorganized neuronal pattern together with a significant increase of glial apoptotic cells, suggesting that glial degeneration likely precedes neuronal demise. Interestingly, a very similar pattern was observed in the brain cortex of a Hunter patient. These observations both *in vitro*, in our model, and *in vivo* suggest that IDS deficit seems to affect the late phases of neurogenesis and/or the survival of mature cells rather than NSC self-renewal. In particular, platelet-derived growth factor receptor- $\alpha$ -positive (PDGFR- $\alpha$ +) glial progenitors appeared reduced in both the IDS-ko NSCs and in the IDS-ko mouse and human Hunter brains, compared with the respective healthy controls. Treatment of mutant NSCs with IDS or PDGF throughout differentiation was able to increase the number of PDGFR- $\alpha$  cells and to reduce that of apoptotic cells to levels comparable to wt. This evidence supports IDS-ko NSCs as a reliable *in vitro* model of the disease, and suggests the rescue of PDGFR- $\alpha$  glial cells as a therapeutic strategy to prevent neuronal degeneration.

Cell Death and Disease (2013) 4, e906; doi:10.1038/cddis.2013.430; published online 7 November 2013

Subject Category: Neuroscience

Mucopolysaccharidosis type II (MPSII or Hunter Syndrome) is a monogenic, X-linked inherited lysosomal storage disorder (LSD) caused by a deficit of the iduronate 2-sulfatase (IDS) enzyme, involved in glycosaminoglycan (GAG) catabolism.<sup>1</sup> The consequent accumulation of GAGs in all cell types induces organ impairment, with incremental neurodegeneration affecting 50–70% of patients. Death generally occurs within 20 years of age.<sup>2</sup> The current therapeutic strategy, enzyme replacement therapy (ERT),<sup>3–5</sup> is effective in peripheral organs but cannot treat brain deterioration because the

recombinant enzyme does not cross the blood–brain barrier. Results in central nervous system treatment have been obtained in MPSII and MPSVII mouse models through different strategies,<sup>6–9</sup> but the translation to humans is hampered by risk of toxicity and immune responses.<sup>10–13</sup> Moreover, late diagnosis, lack of specimens from early symptomatic patients and the absence of *in vitro* models limit the elucidation of the neuro-pathogenetic events involved in the development of Hunter disease. Self-renewing neural stem cells (NSCs), capable of differentiation into neural

<sup>1</sup>Department of Biotechnology and Biosciences, University Milan Bicocca, Piazza della Scienza 2, Milano 20126, Italy; <sup>2</sup>Department of Experimental Oncology, Fondazione IRCCS Istituto Nazionale dei Tumori, Via Amadeo 42, Milano 20133, Italy; <sup>3</sup>Laboratory of Diagnosis and Therapy of Lysosomal Disorders, Department of Women's and Children's Health, University of Padova, Via Giustiniani 3, Padova 35128, Italy; <sup>4</sup>Department of Surgery and Translational Medicine, University Milano Bicocca, Via Cadore 48, Monza 20900, Italy; <sup>5</sup>Casa Sollievo della Sofferenza, Viale Cappuccini 2, San Giovanni Rotondo (FG) 71013, Italy and <sup>6</sup>Stem Cells Laboratory, Cell Factory and Biobank, Azienda ospedaliera "Santa Maria", Terni, Viale Tristano da Joannuccio 1, Terni 05100, Italy

\*Corresponding author: L De Filippis, Department of Biotechnologies and Bioscience, University Milan Bicocca, Piazza della Scienza 2, Milano 20126, Italy; Tel: +39-0264483368; Fax: +39-0264483314; E-mail: lidia.defilippis@unimib.it

<sup>7</sup>These authors contributed equally to this work.

**Keywords:** neural stem cells; MPSII; Hunter Syndrome; glial cells; lysosomal storage disorders

**Abbreviations:**  $\beta$ -tubIII,  $\beta$ -tubulin III; DAPI, 4',6-diamidino-2-phenylindole dihydrochloride; Dcx, double cortin; div, days *in vitro*; ECM, extracellular matrix; EGF, epidermal growth factor; ERT, enzyme replacement therapy; FGF2, fibroblast growth factor type 2; GAG, glycosaminoglycan; GalC, galactocerebroside C; GFAP, glial fibrillary acidic protein; HD, high cell density; IDS, iduronate 2-sulfatase; IDS-ko, IDS-knockout; iPSCs, induced pluripotent stem cells; Lamp1, lysosomal-associated membrane protein 1; LD, low cell density; LSD, lysosomal storage disorder; MAP2, microtubular associated protein type2; MBP, myelin basic protein; MPSVII, mucopolysaccharidosis type VII; NSC, neural stem cell; OBs, olfactory bulbs; PDGF, platelet-derived growth factor; PDGFR, platelet-derived growth factor receptor; SVZ, subventricular zone; wt, wild type

Received 25.6.13; revised 06.9.13; accepted 23.9.13; Edited by A Verkhratsky

phenotypes, create a model for dissecting neurogenesis *in vivo* and for investigating the onset and progression of neurodegenerative diseases *in vitro*.

As the genetic defect in MPSII could compromise the neurogenic properties of NSCs,<sup>14,15</sup> we used NSCs derived from IDS-knockout (IDS-ko) mice to recapitulate MPSII pathogenesis. We also analyzed the relationship between IDS deficit and abnormal neurogenesis *in vivo* to clarify the mechanisms underlying the neuropathology. Our results provide a previously undocumented characterization of the IDS-ko mouse brain mirroring the pattern of a human Hunter brain, indicate glial cell-mediated neurodegeneration as a candidate mechanism involved in MPSII and validate IDS-ko NSCs as a tool to model MPSII neurodegeneration and to investigate novel therapeutic approaches.

## Results

### IDS deficit does not critically affect NSC self-renewal.

We first established two NSC lines from the SVZ of early symptomatic C57BL6 IDS-ko mice and two NSC control lines from wild-type (wt) syngenic littermates. The identity of IDS-ko NSCs was confirmed by PCR (Supplementary Figure 1) and by IDS activity assay (Figure 1a). NSCs were expanded using the neurosphere assay<sup>16,17</sup> and no morphological differences were detectable between wt and IDS-ko neurospheres (Figure 1b). In the presence of both epidermal growth factor (EGF) and fibroblast growth factor type 2 (FGF2), IDS-ko and control NSCs displayed a comparable self-renewal capacity (Figure 1c), and no significant differences were evident between the viability of IDS-ko and control cells at 24, 48 and 72 h from dissociation of the

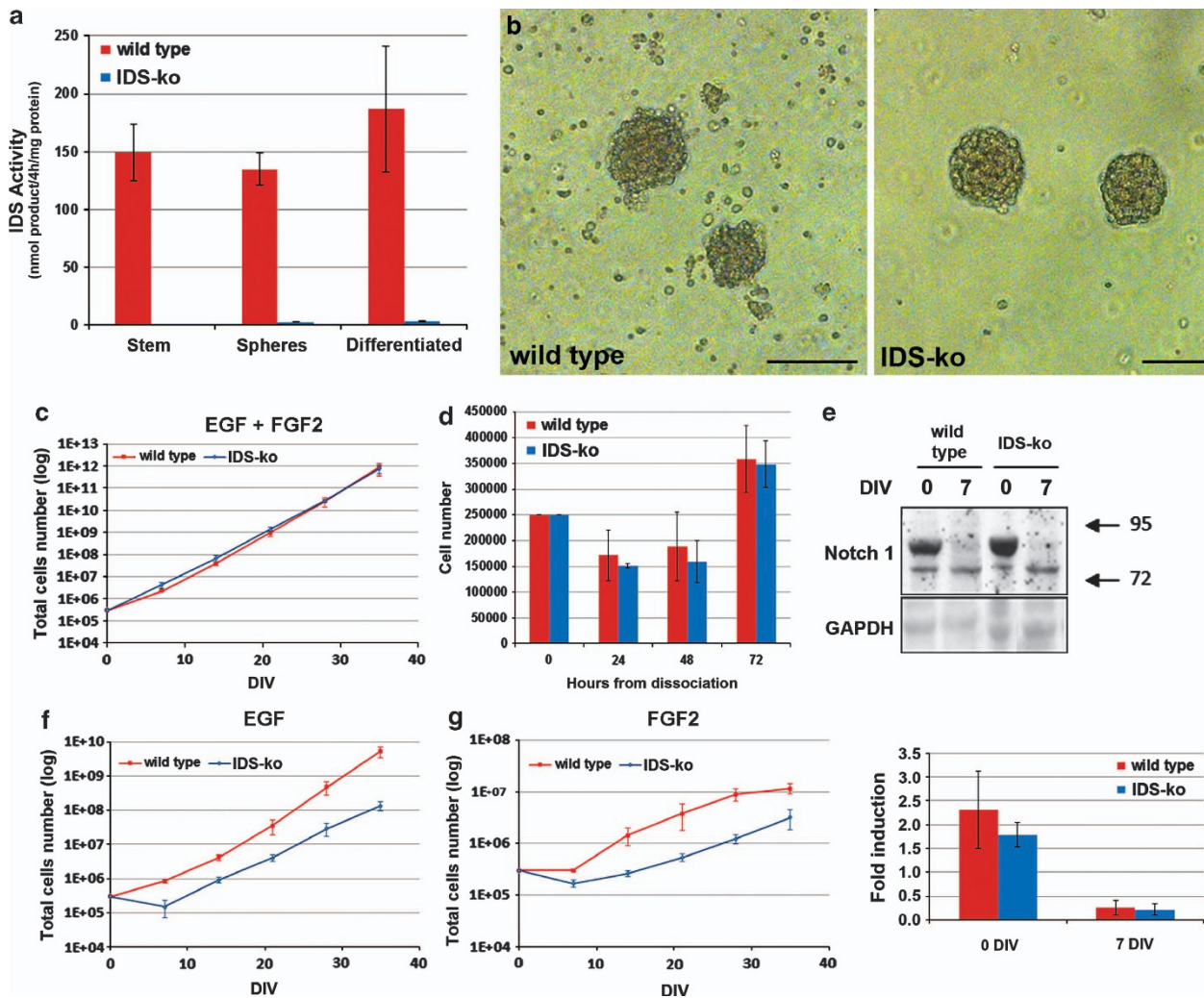


**Figure 1** IDS deficit does not critically affect NSC self-renewal. (a) Histogram showing the IDS enzymatic activity in wt and IDS-ko NSCs. Although detectable in wt single stem cells, neurospheres and differentiated, no enzymatic activity could be revealed in IDS-ko cells. (b) Phase-contrast image of a free floating neurospheres culture. Scale bar: 100  $\mu$ m. (c) Graph showing the proliferation rate of wt NSCs (red,  $n=2$ ) and IDS-ko NSCs (blue,  $n=2$ ) when cultured in the presence of both EGF and FGF2. (d) Histogram showing the number of viable wt and IDS-ko NSCs at 0, 24, 48 and 72 h after dissociation. For each line,  $2.5 \times 10^5$  cells were plated ( $n=2$ ). (e) Western blot analysis of Notch expression in wt and IDS-ko cells at 0 and 7 div after differentiation. (f and g) Graphs showing the proliferation rate of wt NSCs (red,  $n=2$  cell lines) and IDS-ko NSCs (blue,  $n=2$  cell lines) when cultured only in the presence of EGF (f) or in the presence of FGF2 (g). All results are presented as the average of the two IDS-ko and of the two wt NSC lines, respectively. Values are means  $\pm$  S.E.M

neurospheres (Figure 1d). Consistently, the amount of Notch1 protein, crucial for NSC self-renewal, was comparable in wt and in IDS-ko NSCs (Figure 1e). Interestingly, in the absence of either EGF or FGF2, all NSC lines underwent a physiological progressive delay of proliferation, which appeared to be initially enhanced in IDS-ko cells

(Figures 1f and g). These results suggest that IDS expression is not crucial to NSC self-renewal when EGF and FGF2 cooperate to NSC proliferation, but can affect NSC sensitivity to single mitogens possibly by altering the balance between transient amplifying progenitors and stem cells, indicating that IDS may have a role in normal differentiation of NSCs.

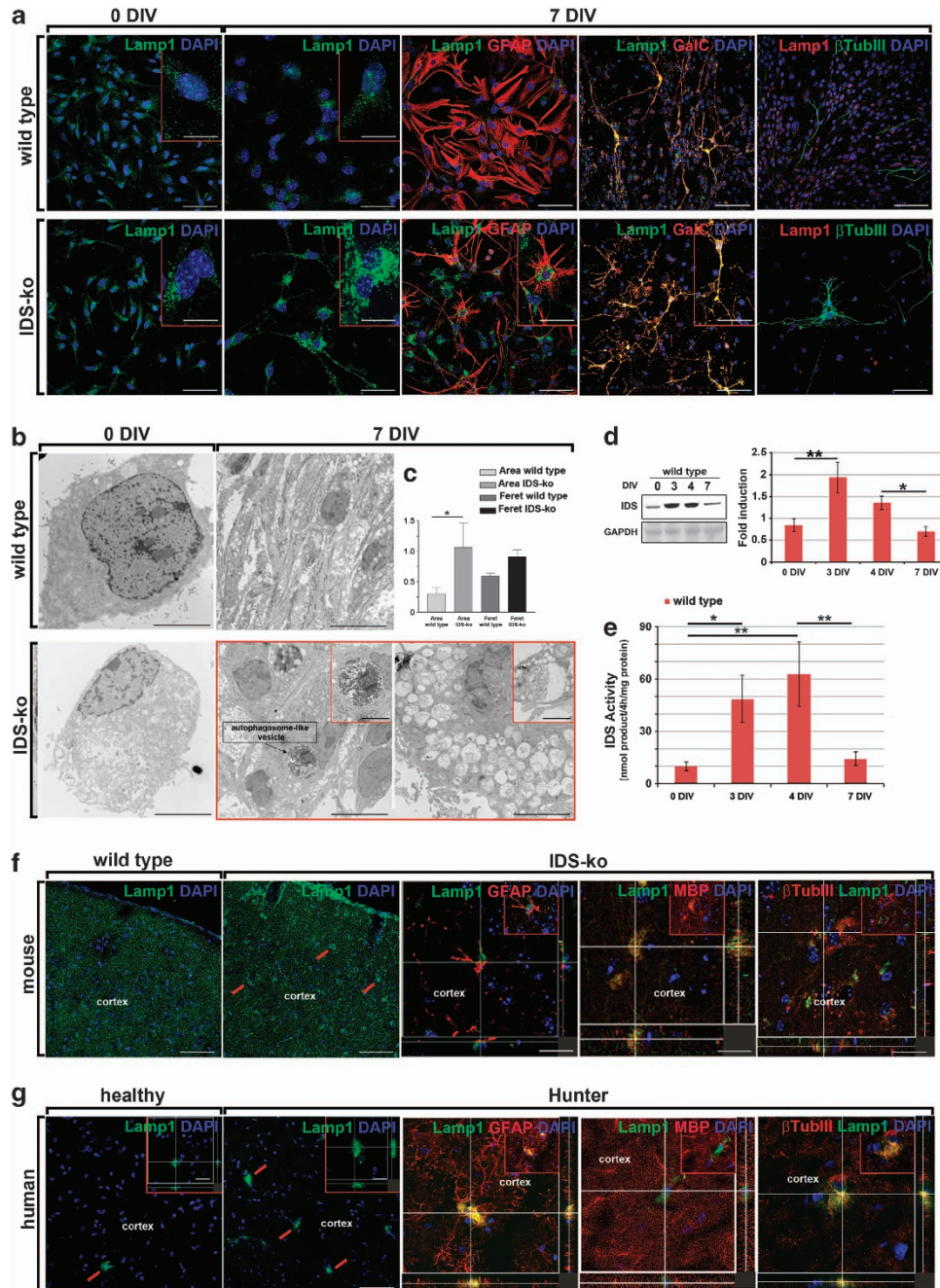


**Figure 2** Lysosomal accumulation in differentiated IDS-ko NSCs and in mature neurogenic areas of both murine and human brains affected by MPSII. (a) Confocal microscopy images of wt and IDS-ko NSCs at 0 div and after 7 div differentiation stained against lysosome marker Lamp1 (scale bar: 10–15  $\mu$ m; inset scale bar: 5–8  $\mu$ m). Scale bars: 75  $\mu$ m; in insets: 11–15  $\mu$ m. (b) Transmission electron microscopy analysis in wt and IDS-ko cells at stem (0 div) and differentiated (7 div) stage. Scale bars: 6  $\mu$ m; in inset: 1.7–2.3  $\mu$ m. (c) Quantification of average lysosomal area and diameter (Ferret) confirmed the presence of macro-lysosomal organelles in IDS-ko differentiated cells. Values are means  $\pm$  S.E.M. (d and e) Western blot analysis (d) and enzymatic activity assay (e) of IDS in wt cells at 0, 3, 4 and 7 div. The differences among all the values were statistically not significant unless indicated (\* $P \leq 0.05$ , \*\* $P \leq 0.01$ , \*\*\* $P \leq 0.001$ ); Student's *t*-test for all experiments was applied. (f) Confocal microscopy images of wt and IDS-ko mouse brain cortex stained against Lamp1. Scale bars: 75  $\mu$ m. Zoomed images scale bars: 11–15  $\mu$ m. (g) Confocal microscopy images of brain cortex from a healthy and Hunter patient stained against Lamp1. Scale bars: 75  $\mu$ m; in inset: 17–25  $\mu$ m. Zoomed images scale bars: 15–31  $\mu$ m

**Lysosome anomalies increase with differentiation.** To determine whether GAG accumulation because of IDS deficit could hamper normal differentiation of IDS-ko NSCs, we evaluated lysosomal aggregation as a pathological hallmark correlated with GAG accumulation. We investigated the expression of the lysosomal marker lysosomal-associated membrane protein 1 (Lamp1) both *in vitro* during differentiation and *in vivo*, in the IDS-ko mouse brain and in human Hunter cortex. Although only incipient at the undifferentiated stage (Figure 2a, 0 days *in vitro* (div)), a massive accumulation of Lamp1+ lysosomal organelles was evident after 7 days of differentiation in IDS-ko cells (Figure 2a, 7 div). In particular, the lysosomal accumulation colocalized with glial fibrillary acidic protein+ (GFAP+) astrocytes and galactocerebroside C+ (GalC+) oligodendrocytes, and only occasionally with  $\beta$ -tubulin III+ ( $\beta$ -tubIII+) neurons (Figure 2a), suggesting that IDS deficit primarily affects glial cells. Consistently, analysis by transmission electron microscopy showed that undifferentiated IDS-ko NSCs displayed sporadic multivesicular bodies (Figure 2b, 0 div) that were absent in wt NSCs (Figure 2b, 0 div), and these lysosomal anomalies appeared to exacerbate over differentiation (Figure 2b, 7 div). IDS-ko cells displayed massive vacuolization (inset in Figure 2b, 7 div bottom center and right) and aberrant autophagosome-like vesicles (inset in Figure 2b, bottom right), whereas wt cells maintained a normal pattern (Figure 2b, upper center). Average lysosomal area in IDS-ko differentiated cells was  $1.07 \mu\text{m}^2 \pm 0.40$  versus  $0.30 \mu\text{m}^2 \pm 0.10$  in wt cells ( $P \leq 0.05$ ), with, respectively, a maximal Feret diameter of  $0.91 \mu\text{m} \pm 0.11$  versus  $0.59 \mu\text{m} \pm 0.05$  (Figure 2c). We next investigated how IDS expression is normally regulated during differentiation. IDS protein level (Figure 2d) in wt NSCs correlated with enzymatic activity (Figure 2e) and peaked at 3 div, a checkpoint when most NSCs are committed progenitors, and decreased with terminal differentiation. This suggests that IDS deficit induces precocious differentiation of NSCs conditioning long-term survival of transient progenitors. We then analyzed the *in vivo* samples. In wt animals, lysosomes were homogeneously distributed throughout the brain and no aberrant accumulation was detectable (Figure 2f). Consistent with the *in vitro* results, lysosomal aggregation appeared incipient in glial cells of IDS-ko mouse brains at an early symptomatic stage (p42; Supplementary Figure 3).

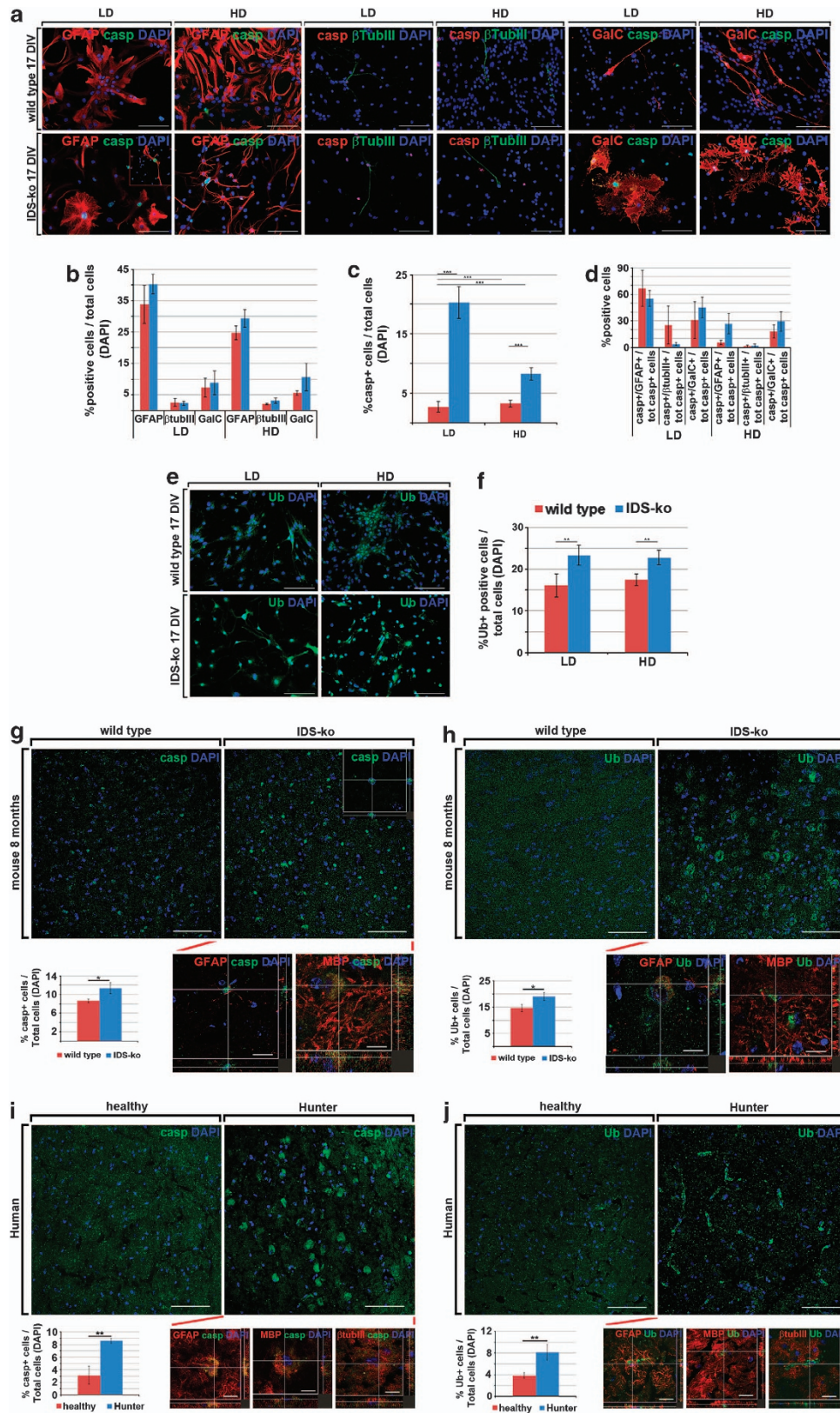
At symptomatic stage (8 months), Lamp1+ lysosomal aggregates were particularly evident in mature brain areas such as cortex (Figure 2f), striatum, septum and olfactory bulbs (OBs), while less evident in the stem niche of the SVZ (Supplementary Figure 2) and mostly colocalizing with GFAP+ astroglial cells and myelin basic protein+ (MBP+) myelin fibers (Figure 2f, zoomed images). No  $\beta$ -tubIII+ cells displayed abnormal lysosomal patterns (Figure 2f, zoomed image) until the end stage (11 months; Supplementary Figure 3). Interestingly, an analogous pattern was observed in the brain cortex of a Hunter patient (Figure 2g). In the healthy human brain (Figure 2g, healthy), only sporadic cells with evident lysosomal aggregation could be detected. In these cells, Lamp1+ organelles displayed a chain-like morphology (Figure 2g, inset in healthy), whereas in the Hunter brain they appeared clustered and distributed throughout the cytosol (Figure 2f, inset in Hunter). These findings suggest IDS-ko NSCs as a valid tool to mimic MPSII pathology and glial degeneration as possibly preceding and contributing to later neuronal death.

### Pathological differentiation and apoptosis of IDS-ko NSCs is cell-density dependent.

Previous studies on neural progenitor cells from MPSVII mice showed that GAG accumulation because of  $\beta$ -glucuronidase deficiency does not alter neuronal differentiation.<sup>18</sup> To assess whether lysosomal accumulation in IDS-ko glial cells could alter neuronal and/or glial differentiation or maturation, we investigated the differentiation potential of wt and IDS-ko NSCs. We first analyzed the expression of the stem-related marker nestin. The reduction of nestin+ cells during differentiation appeared accelerated in IDS-ko cells with respect to wt (Supplementary Figures 3A and B): at 0 div, IDS-ko and wt neurospheres contained comparable percentages of nestin+ NSCs, whereas at 7 div the number was significantly lower in IDS-ko cells (Supplementary Figure 3B).

We then evaluated the expression of later neuronal and glial markers:  $\beta$ -tubIII and microtubule-associated protein 2 (MAP2) in neurons, GalC in oligodendrocytes and GFAP in astrocytes. In accordance with the rapid decrease of nestin+ cells, we observed that, at 0 div, IDS-ko NSCs displayed a precocious expression of neuronal and oligodendroglial markers (Supplementary Figures S3C–G,I,J). Moreover, at 7 div, a higher percentage of  $\beta$ -tubIII+ neuronal cells and of

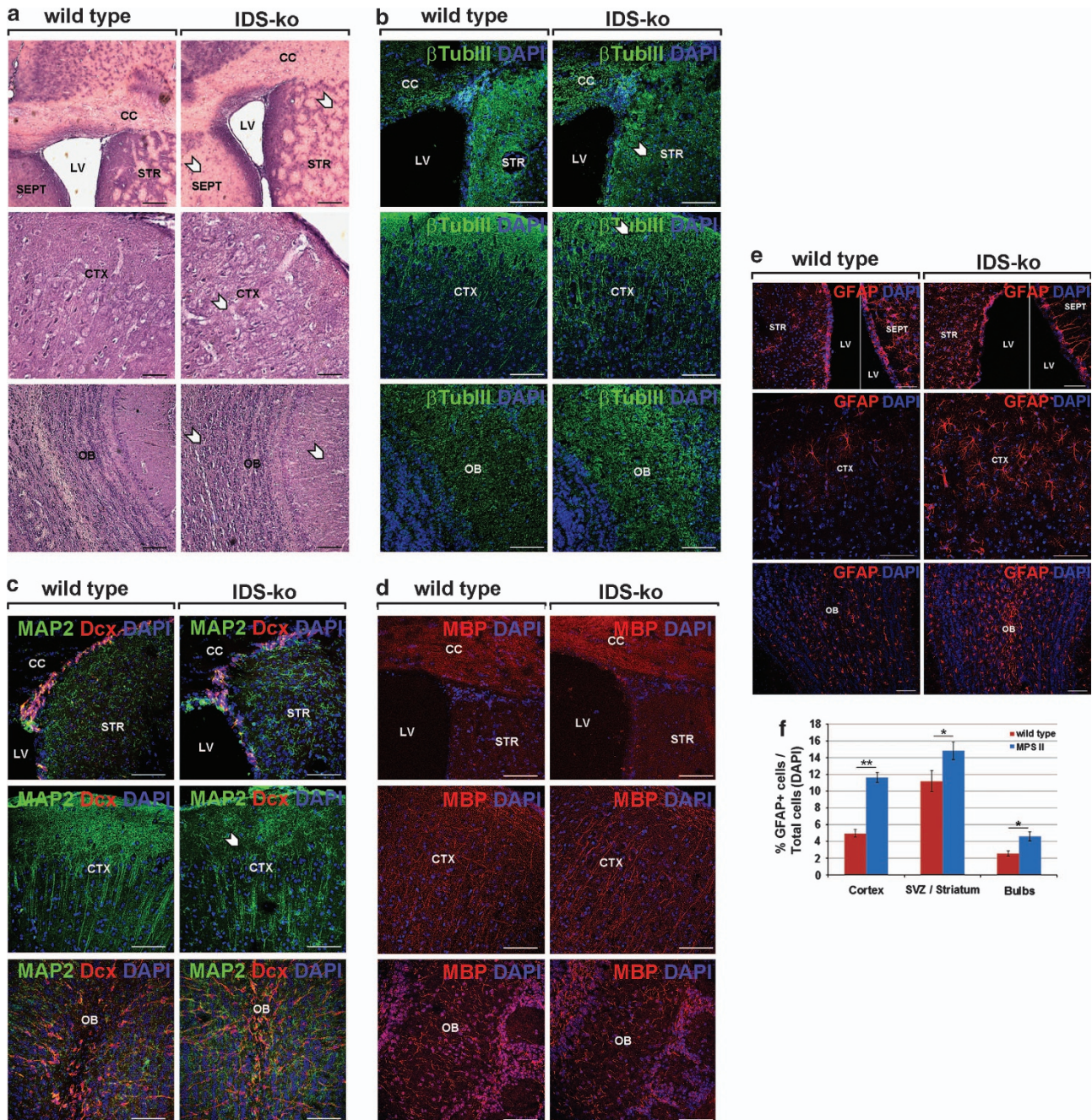
**Figure 3** Effect of cell density over IDS-ko NSCs differentiation. (a–f) Coimmunostaining for caspase3+ and ubiquitin with the neural differentiation markers  $\beta$ -tubIII, GFAP and GalC of wt and IDS-ko NSCs at 0 and 17 div of differentiation under HD ( $1.25 \times 10^4$  cells/cm<sup>2</sup>) and LD ( $6.5 \times 10^3$  cells/cm<sup>2</sup>) cell density conditions. (a) Confocal microscopy images showing the coimmunostaining of caspase3 marker with GFAP, GalC or  $\beta$ -tubIII under HD or low LD conditions. Scale bar: 100  $\mu\text{m}$ . (b) Quantification of GFAP+,  $\beta$ -tubIII+ and GalC+ cells over total DAPI+ nuclei under HD and LD conditions. (c) Quantification of caspase3+ cells over total DAPI+ nuclei under HD and LD conditions. (d) Quantification of GFAP+/caspase3+,  $\beta$ -tubIII/caspase3+, GalC+/caspase3+ cells over total caspase3+ cells under HD and LD conditions. (e) Confocal microscopy images showing the immunostaining of ubiquitin+ marker. Scale bar: 100  $\mu\text{m}$ . (f) Quantification of ubiquitin+ cells over total DAPI+ nuclei under HD and LD conditions. (g) Confocal microscopy images showing the presence of caspase3+ cells in wt (upper left) and IDS-ko (upper right) mouse cortex. Scale bar: 75  $\mu\text{m}$ ; in inset: 11.72  $\mu\text{m}$ . Quantification of caspase3+ cells over total DAPI+ nuclei (bottom left) and colocalization with glial markers GFAP (bottom center) and MBP (bottom right). Scale bars: 21, 10  $\mu\text{m}$ . (h) Confocal microscopy images showing the presence of ubiquitin+ cells in wt (upper left) and IDS-ko (upper right) mouse cortex. Scale bar: 75  $\mu\text{m}$ . Inset scale bar: 16  $\mu\text{m}$ . Quantification of ubiquitin+ cells over total DAPI+ nuclei (bottom left) and colocalization with GFAP (bottom center) and MBP (bottom right). Scale bar: 13.7  $\mu\text{m}$ . (i) Confocal microscopy images showing the presence of caspase3+ cells in wt (upper left) and Hunter (upper right) human cortex (end stage). Scale bar: 75  $\mu\text{m}$ . Quantification of caspase3+ cells over total DAPI+ nuclei (bottom left) and colocalization with GFAP (bottom center), MBP (bottom right) and neuronal marker  $\beta$ -tubIII (bottom right). Scale bar: 10–14  $\mu\text{m}$ . (j) Confocal microscopy images showing the presence of ubiquitin+ aggregates in wt (upper left) and Hunter (upper right) human cortex (end stage). Scale bar: 75  $\mu\text{m}$ . Quantification of caspase3+ cells over total DAPI+ nuclei (bottom left) and colocalization with GFAP (bottom center), MBP (bottom right) and  $\beta$ -tubIII (bottom right). Scale bars: 16–18  $\mu\text{m}$ . Student's *t*-test was applied, the differences among all the values were statistically not significant unless indicated (\* $P \leq 0.05$ , \*\* $P \leq 0.01$ , \*\*\* $P \leq 0.001$ ) values are means  $\pm$  S.E.M. Casp, active caspase 3; Ub, ubiquitin



GalC + oligodendrocytes was present in IDS-ko NSC-derived progeny compared with wt control (Supplementary Figures 3C, D, I and J), with a decrease of GFAP + cells (Supplementary Figures 3C and D). The morphology of IDS-ko cells also appeared more differentiated with respect to the wt counterparts (Supplementary Figures 3C, F and I),

with evidence of emerging processes at 0 div (Supplementary Figures 3C, F and I, white arrows) becoming long and branching at 7 div.

These observations suggest that IDS-ko NSCs retain multipotency, but display an inherent bias to precocious differentiation and/or maturation, leading to suppose that



GAG accumulation deriving from IDS deficit could lead to an accelerated neurogenetic process *in vivo* and ensuing precocious apoptosis of neural cells. To test this hypothesis *in vitro*, we forced long-term differentiation under low cell density (LD) conditions ( $6.5 \times 10^3$  cells/cm<sup>2</sup>). At 17 div, IDS-ko cells spontaneously originated a lower number of oligodendrocytes with respect to cells cultured under high cell density (HD) conditions ( $2.5 \times 10^4$  cells/cm<sup>2</sup>) (Figures 3a and b). We next investigated the number of active caspase3+ cells to assess whether IDS-ko differentiated cells undergo precocious apoptosis. At 17 div, under HD, a significantly higher percentage of IDS-ko differentiated cells was caspase3+ ( $8.21 \pm 1.03\%$ ) with respect to wt cells ( $3.19 \pm 0.53\%$ ,  $P \leq 0.001$ ) (Figure 3c). This effect appeared further enhanced at LD, where the number of mutant apoptotic cells raised to  $20.26 \pm 2.72\%$  compared with  $2.65 \pm 0.87\%$  ( $P \leq 0.001$ ) of wt apoptotic cells (Figure 3c). Interestingly, under both HD and LD, most of caspase3+ cells were GFAP+ astrocytes and GalC+ oligodendrocytes in IDS-ko cells (Figure 3d).

Similar results were obtained by the analysis of ubiquitin aggregates, which are associated to apoptosis-related catabolism of degradation products.<sup>19</sup> Unlike wt cells, mutant cells displayed a heterogeneous distribution of ubiquitin, which appeared concentrated in the perinuclear area and showed irregular protein aggregates under HD and LD (Figures 3e and f).

To correlate the *in vitro* analysis with the pathology in the animal model, we investigated the number of caspase3+ cells and the presence of ubiquitin aggregates *in vivo*. In the IDS-ko mouse, we found an incipient lysosomal aggregates at early symptomatic stage (Supplementary Figure 4) and a significantly higher percentage of caspase3+ cells and of ubiquitin+ aggregates with respect to wt in the cortex and striatum at symptomatic stage (Figures 3g and h). On the contrary, no remarkable differences were detectable in the SVZ of mutant and wt animals (Supplementary Figure 4A). Importantly, caspase3+ cells and ubiquitin aggregates mostly colocalized with GFAP (zoomed images in Figure 3g) or MBP (zoomed images in Figure 3h) glial markers, whereas not with the neuronal marker  $\beta$ -tubIII+. The presence of neuronal apoptotic cells was evident only at later stages (Supplementary Figure 4B),<sup>20</sup> suggesting that degeneration of glial cells precedes that of neuronal cells in an age-dependent manner.

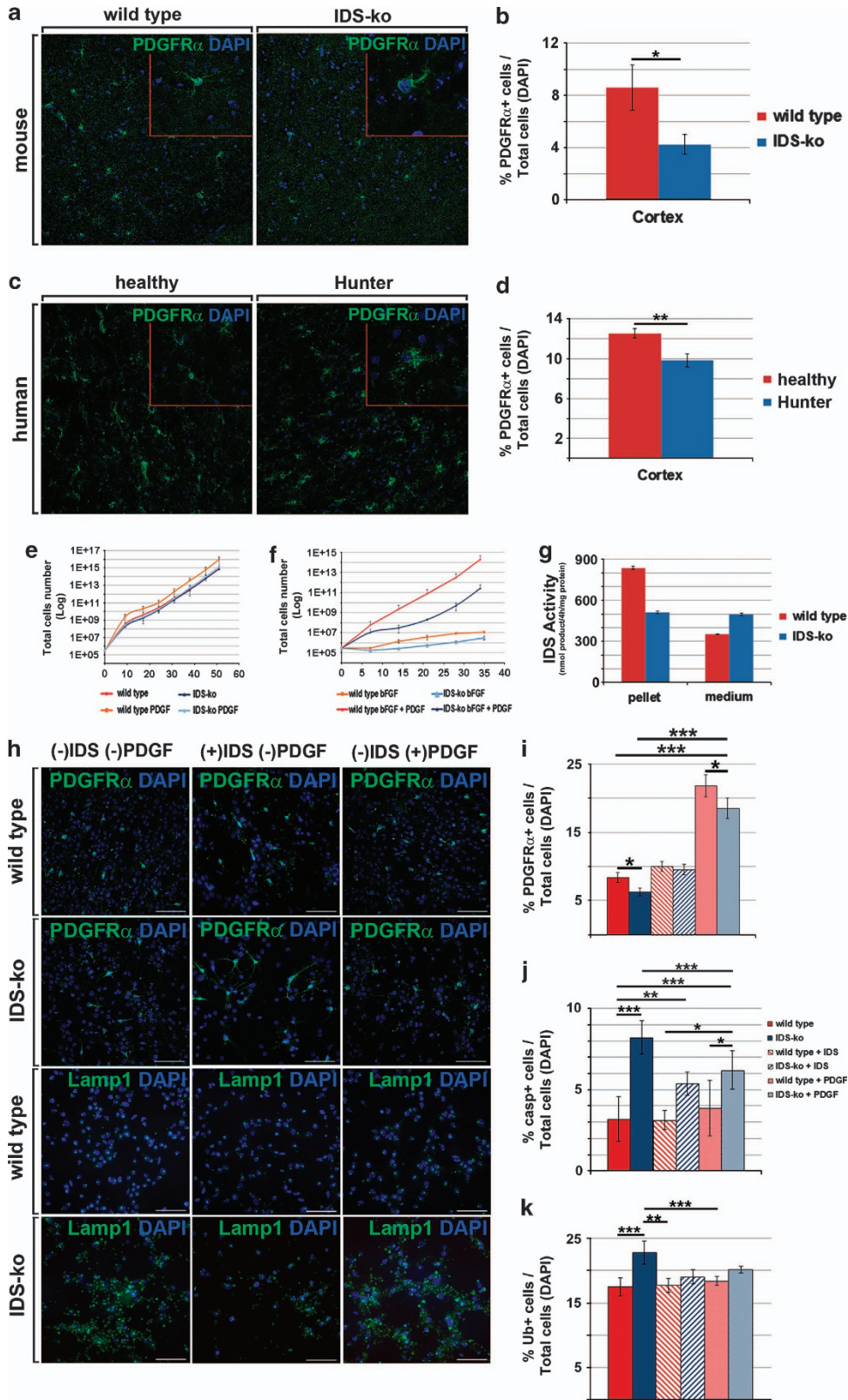
The results obtained were consistent with those from the analysis of the Hunter patient (Figures 3i and j). The fraction of caspase3+ and of ubiquitin+ cells in the Hunter cortex was higher ( $P \leq 0.01$ ) than in the wt brain (Figures 3i and j). GFAP+, MBP+ and  $\beta$ -tubIII+ cells were identified as colabeled with caspase3 (zoomed images in Figure 3i) or ubiquitin (zoomed images in Figure 3j) antibodies, confirming the presence of both glial and neuronal degeneration at the terminal point (death) of disease progression in humans. On the contrary, no differences were observed between healthy and Hunter SVZs. Although we cannot exclude that other regulatory processes independent of NSC biology, such as neuroinflammation, may be responsible for the observed neurodegeneration, these results suggest an important involvement of glial cells in MPSII pathology.

**IDS deficit affects mature brain areas.** We next sought to determine to what extent the neurogenic pattern is hampered in IDS-ko mouse brain. A preliminary hematoxylin-eosin histochemical analysis revealed loose and disorganized tissue architecture in the striatum, septum, corpus callosum, cortex and OBs of IDS-ko mice (Figure 4a). Unlike the regular and homogeneous distribution of neuronal cells in the mature brain areas of wt animals, both  $\beta$ -tubIII+ (Figure 4b) and MAP2+ (Figure 4c) neuronal cells were chaotically intermingled in IDS-ko mouse brains, although the number of NeuN+ cells remained unaltered (not shown). To exclude that a lower number of early neuronal progenitor cells could account for the poor neurogenesis, we investigated the expression of double cortin (Dcx), a neuronal progenitor marker. Although only sporadically detectable in cortex and striatum, Dcx+ cells appeared numerous in the OBs and in the SVZ of IDS-ko brains (Figure 4c), but their number and morphology did not appear significantly different from wt. Indeed, the SVZ regions of IDS-ko and wt mice appeared indistinguishable (Supplementary Figure 2), supporting the hypothesis that GAG metabolism has no significant influence on NSC self-renewal or early differentiation neither *in vitro* nor *in vivo*. When analyzing the myelin pattern, MBP+ cells in IDS-ko mice displayed a disorganization complementary to that of neuronal cells (Figure 4d), but no evident reduction of MBP was detectable by densitometric analysis. On the contrary, we observed a remarkable increase of activated GFAP+ cells in the IDS-ko brain (Figures 4e and f).

A similar patterning was observed in the human cortex from an end-stage Hunter patient (Supplementary Figure 5).

#### **IDS deficit induces degeneration of platelet-derived growth factor receptor- $\alpha$ -positive (PDGFR $\alpha$ + ) progenitors.**

After observing that astroglial GFAP+ cells were more numerous and morphologically reactive in IDS-ko *versus* wt brains (Figures 4e and f), we investigated the number and distribution of PDGFR $\alpha$ + neural progenitors, which appeared reduced and with a remarkably altered morphology in the brain of mutant mice (Figure 5b). Although normal PDGFR $\alpha$ + cells presented a small cell body with long processes, mutant cells appeared fibrotic and amoeboid with short branching (Figure 5a). To exclude that this could depend on defective neurogenesis from the SVZ, we counted the number of PDGFR $\alpha$ + cells in the SVZ of mutant and wt mice and detected no differences. Interestingly, a very similar pattern was present in the cortex of the Hunter patient (Figure 5c), where the number of PDGFR $\alpha$ + cells was reduced with respect to the control (Figure 5d), whereas the healthy and Hunter SVZs appeared undistinguishable. Following these observations, we translated the analysis to the IDS-ko NSCs. When PDGF was added to the culture medium to potentiate the proliferation of PDGFR $\alpha$ + cells,<sup>21</sup> mutant neurospheres showed a more modest growth rate enhancement than wt NSCs (Figure 5e). This divergence appeared further enhanced after removal of EGF, a condition that privileges the expansion of PDGFR $\alpha$ -responsive cells (Figure 5f). Effects obtained from PDGF treatment were compared with the addition of recombinant IDS from expansion throughout differentiation. Enzyme activity assay confirmed that the IDS enzyme was taken up by mutant cells



and was functionally active (Figure 5g). We observed an increase of PDGFR $\alpha$ <sup>+</sup> progenitors and a reduction of Lamp1<sup>+</sup> aggregates in IDS-treated IDS-ko NSCs and to a lesser extent after PDGF treatment (Figure 5h). We evaluated the number of PDGFR $\alpha$ <sup>+</sup>, caspase3<sup>+</sup> and ubiquitin<sup>+</sup> cells in untreated, IDS- and PDGF-treated cells after 17 div (Figures 5i–k). Interestingly, the fraction of PDGFR $\alpha$ <sup>+</sup> cells was remarkably increased in MPSII cultures treated with either IDS or PDGF with respect to untreated controls (Figure 5i). In wt cells, a similar increase of PDGFR $\alpha$ <sup>+</sup> cells was obtained by treatment with PDGF, whereas no significant differences were evident between untreated and IDS-treated cells (Figure 5i).

In accordance with the partial rescue of PDGFR $\alpha$ <sup>+</sup> cells, the number of caspase3<sup>+</sup> apoptotic cells in IDS-ko NSC-derived progeny was significantly decreased by both IDS and PDGF treatments compared with untreated cells (Figure 5j).

Similarly, the percentage of mutant cells displaying ubiquitin aggregates was dampened by IDS treatment (Figure 5k), whereas PDGF treatment did not induce significant effects (Figure 5k).

These results suggest the involvement of PDGF signaling in MPSII pathogenesis and that treatment with PDGF could contribute to ameliorate the pathological environment, although it does not suffice for the complete rescue of the pathology.

## Discussion

With the aim to recapitulate the pipeline of MPSII neuropathology, we analyzed the differentiation pattern of NSCs derived from the SVZ of early symptomatic IDS-ko mice in comparison with a time-course analysis of MPSII mouse brains at different stages of the disease and with a human Hunter cortex. Consistent with previous studies,<sup>18</sup> mutant NSCs displayed a self-renewal capacity comparable to wt NSCs, suggesting that IDS activity is not crucial for stem cell metabolism or to maintain a stable self-renewal. However, their dependence on the removal of mitogens from the culture medium was initially remarkably higher, suggesting that IDS deficit could hamper normal differentiation. Indeed, during differentiation, IDS-ko NSCs displayed an increasing and robust accumulation of lysosomal organelles, which was absent in normal cells. Interestingly, both IDS expression and activity in normal cells peaked at the progenitor stage leading to speculate that IDS could prime the correct commitment of transient progenitors and/or contribute to establish an

extracellular environment suitable to functional differentiation and survival of mature cells.

Consistently, the precocious expression of neuronal and glial markers in mutant NSCs was accompanied by the rapid achievement of a specialized morphology and followed by an increase of apoptotic cells, suggesting a quicker differentiation of IDS-ko NSC, which was enhanced by stringent culture conditions (LD). In particular, most lysosomal aggregates were detected in glial cells *in vitro* and a comparable patterning could be observed in IDS-ko mouse brains, suggesting that late neuronal degeneration *in vivo* (11 months aged IDS-ko mouse brain and human Hunter's brain)<sup>20</sup> could depend on a primary degeneration of non-neuronal cells. It must be considered that various mechanisms are involved in LSD pathogenesis.<sup>22</sup> Accumulation in the extracellular matrix (ECM) of heparan- and dermatan-sulfate fragments with altered sulphation pattern could affect signal transduction pathways, as previously described in MPSI.<sup>23</sup> This could hinder the development of appropriate cell–cell contacts between neuronal and oligodendroglial or astroglial cells, which have a key role in driving correct neurogenetic processes. In accordance with this hypothesis, we observed that under LD conditions, precocious differentiation and apoptosis of IDS-ko NSC-derived progeny were enhanced. Indeed, Lemonnier *et al.*<sup>15</sup> recently demonstrated that gene expression profiling in NSCs derived from MPSIIIB induced pluripotent stem cells (iPSCs) shows dramatic alterations of ECM components and of cell–matrix interactions. In this view, we cannot exclude that early cell apoptosis could depend on other reasons aside from developmental programming and the analysis of ECM in Hunter's brain would deserve further attention in future studies.

In parallel with *in vitro* studies, we investigated the integrity of the neural tissue and performed a detailed characterization of the IDS-ko mouse brain. Many lysosomal and ubiquitin aggregates were present in the IDS-ko brain parenchyma together with a disorganized cytoarchitecture and a significant number of apoptotic cells, mostly GFAP<sup>+</sup> astrocytes and MBP<sup>+</sup> oligodendrocytes, supporting our hypothesis that neuronal degeneration follows glial cell death.<sup>20</sup> This pattern was consistent with the evidence from IDS-ko NSC differentiation *in vitro* and, importantly, mirrored that of the brain cortex of an end-stage MPSII patient, except for the fact that the human cortex displayed the presence of both glial and neuronal apoptotic cells, similar to the pattern of end-stage IDS-ko mice.<sup>20</sup> The lack of human samples hampered the analysis at earlier stages of the disease, but our observation is

**Figure 5** IDS deficiency affects the number of PDGFR $\alpha$ <sup>+</sup> progenitors both in mouse and in human: potential therapeutic effects of PDGF. (a) Confocal microscopy images of wt and IDS-ko mice brain cortex immunostained for the glial PDGFR $\alpha$  marker. Scale bar: 75  $\mu$ m. Inset images show the difference between the wt long-branching and the mutant round-shaped morphologies of PDGFR $\alpha$ <sup>+</sup> cells. Scale bars: 26  $\mu$ m in wt and 8  $\mu$ m in IDS-ko. (b) Quantification of PDGFR $\alpha$ <sup>+</sup> cells over total DAPI<sup>+</sup> cells. (c) Confocal microscopy images of wt and Hunter human cortex immunostained for the glial PDGFR $\alpha$  marker. Scale bar: 75  $\mu$ m. Inset images show the difference between the wt long-branching and the mutant disrupted morphologies of PDGFR $\alpha$ <sup>+</sup> cells. Scale bars: 22  $\mu$ m in healthy and 11  $\mu$ m in Hunter. (d) Quantification of PDGFR $\alpha$ <sup>+</sup> cells over total DAPI<sup>+</sup> cells. (e and f) Graphs showing the proliferation rate of wt NSC (red, orange) and IDS-ko NSC (blue, light blue) when cultured in the presence of both EGF and FGF2 (E) or FGF2 alone (f) with or without addition of PDGF. (g) Enzymatic IDS activity assay in wt and IDS-ko murine NSCs and related supernatants after addition of IDS to the culture medium for 5 div, showing the rescue of IDS activity in IDS-ko cells. (h) Confocal microscopy images of wt and IDS-ko NSCs cultured and differentiated for 10 div with or without addition of IDS or PDGF to the culture media and immunostained with antibodies against PDGFR $\alpha$  and Lamp1. (i–k) Histograms showing the percentage of PDGFR $\alpha$ <sup>+</sup> (i), Caspase 3<sup>+</sup> (j) and ubiquitin<sup>+</sup> (k) cells over total nuclei in untreated, PDGF- or IDS-treated wt and IDS-ko NSCs differentiated for 10 div. The differences among all the values were statistically not significant unless indicated (\* $P \leq 0.05$ , \*\* $P \leq 0.01$ , \*\*\* $P \leq 0.001$ ); Student's *t*-test was applied for b, d and g, whereas one-way ANOVA followed by Student's *t*-test for i, j and k experiments

consistent with late neuronal damage driven by glial degeneration. Hence, although not further explored and beyond the aim of this study, epigenetic modifications could be assumed to have a role in MPSII, and will be addressed in future studies to elucidate the involvement of specific proteins or molecules such as neurotrophic factors, ECM components and chemoattractants.<sup>24,25</sup>

In this view, the use of NSCs derived from IDS-ko mice for modeling MPSII pathogenesis holds great promise, although it is not flawless: a number of mechanisms which underpin MPSII pathogenesis are likely related to the central nervous system microenvironment and non-neural cell-mediated and may not be recapitulated by NSC modeling *in vitro*, such as chronic inflammation.<sup>22</sup> In the same areas with major lysosomal aggregation and tissue disorganization, we found a dramatic increase of fibroblast-like astrocytes, entailing that astrogliosis was concomitant with an evolving inflammatory environment.

A recent study<sup>26</sup> showed that two distinct subsets of progenitors coexist in the SVZ: GFAP-expressing NSCs and PDGFR $\alpha$ -expressing progenitors. In our study, conversely to GFAP+ cells, we observed a defective pool of PDGFR $\alpha$ + progenitors in the cortex of IDS-ko mouse brain and of the human Hunter patient. Whether the defective pool of PDGFR $\alpha$ + neural progenitors is due to a deficient generation from NSCs in the SVZ, to a dysregulation of the PDGF/PDGFR autocrine loop<sup>21</sup> or to other secondary pleiotropic effects during neurogenesis, has still to be definitely shown. As no alterations were evident in the SVZ, our data tend to exclude the first hypothesis. However, these observed changes also occurred *in vitro* in our model system. Mutant NSCs generated a lower fraction of PDGFR $\alpha$  progenitors *in vitro* than wt cells and this impairment was reverted by IDS treatment, similar to what ERT does *in vivo*, thus supporting NSCs as a tool to model MPSII *ex vivo*. Moreover, the addition of PDGF to IDS-ko NSCs partially mimicked the effects of the IDS enzyme suggesting PDGF, already known to bind GAGs and differentially regulate their mitogenic function,<sup>27,28</sup> as involved in the survival of neural progenitors in a LSD disease.

Unlike recent evidence of defective self-renewal of iPSCs from MPSVII patients,<sup>29</sup> in our study IDS deficit appears not to affect NSC proliferation, thus entailing that brain development during the embryonic stage may be normal. The characterization of the IDS-ko adult mouse brain and the unique parallelism with the analysis of a human Hunter brain strengthen our findings, emphasizing their clinical relevance and the reliability of the IDS-ko animal model for neuropathogenic evaluations.

This is the first report suggesting abnormal NSC-derived glial progenitor differentiation as a potential mechanism for the development of MPSII neuropathology and we were able to modulate the mutant phenotype of IDS-ko NSCs *in vitro* by ERT or PDGF treatment, thus fostering NSCs as a valid tool for drug screening and PDGF as a candidate molecule for a combined therapeutic approach to MPSII. On the basis of our results, we propose the transplantation of NSC-derived glial progenitors, or the injection of PDGF and other gliotrophins combined with ERT, among the strategies for future clinical applications.<sup>30</sup>

## Materials and Methods

**Mice.** C57BL6 IDS-ko mice were kindly provided by J Muenzer (University of North Carolina, NC, USA), C57BL6 wt mice were purchased from Harlan Italy (Milano, Italy). ko and wt mice were housed in light- and temperature-controlled conditions, with food and water provided *ad libitum*. All animal care and experimental procedures were conducted according to the current national and international animal ethics guidelines.

**Human specimen.** Human tissue was obtained from the NIHCD Brain and Tissue Bank for Developmental Disorders at the University of Maryland, Baltimore, MD, USA (UMB#M1987 for Hunter's sample; UMB#5387 for the age-matched healthy control).

**Propagation and differentiation of mouse NSCs.** Two wt and two IDS-ko neural stem cell lines were isolated and propagated from the SVZ of adult mouse brains at 6–7 weeks of age as described by Vescovi *et al.*<sup>31</sup> Here all results will be presented as the average of the two IDS-ko and of the two wt NSC lines, respectively.

**Differentiation of NSCs.** To induce NSC differentiation, individual spheres were mechanically dissociated and cells were transferred at  $2.5 \times 10^4$  cells/cm<sup>2</sup> (high-density conditions) or  $6.5 \times 10^3$  cells/cm<sup>2</sup> (low-density conditions) onto cultrex-coated chamber-slides and differentiated as described in Gritti *et al.*<sup>32</sup> for a total of 7 or 17 days. Where indicated, cells were treated throughout differentiation with PDGF (20 ng/ml; Peprotech, Rocky Hill, NJ, USA) or IDS enzyme (4  $\mu$ g/ml). Human recombinant IDS was obtained as a pool of residual microvolumes following patients administration.

**Generation of growth curves.** The rate of expansion of the NSCs was obtained by plating  $3 \times 10^5$  cells in separate T25 flasks in growth medium containing FGF2 (20 ng/ml) and EGF (10 ng/ml; Peprotech) and PDGF (20 ng/ml; Peprotech) in different combinations where indicated. At each passage (p), NSC-originated neurospheres were dissociated the total cell number was calculated on the basis of amplification rate at each passage; the logarithmic value of the total viable-cell number was plotted against the div, starting from the beginning of the experiment. For each condition, growth curves were performed in duplicate.

**Immunocytochemistry.** Cultures were fixed in freshly prepared, buffered 4% paraformaldehyde. After blocking with 10% normal goat serum, cultures were incubated overnight at 4 °C with the following antibodies (monoclonal antibody, monoclonal; polyclonal antibody, polyclonal): nestin (monoclonal, MAB 353, Millipore, Bedford, MA, USA; 1:200, Species Cross Reactivity: mouse, rat),  $\beta$ -tubIII (monoclonal, MMS-435P, Covance, Princeton, NJ, USA; 1:400, Species Cross Reactivity: mammalian), GFAP (polyclonal, Dako, Glostrup, Denmark; 1:400, Species Cross Reactivity: mammalian), GalC (monoclonal, MAB345, Chemicon - Millipore Bioscience Research Reagents, Temecula, CA, USA; 1:100, Species Cross Reactivity: bovine, human, mouse, rat, rabbit), Lamp1 (polyclonal, ab24170, Abcam, Cambridge, UK; 1:750, Species Cross Reactivity: dog, human, mouse, rat, Zebrafish), caspase3 (Asp 170) (polyclonal, #9961, Cell Signaling, Danvers, MA, USA; 1:500, Species Cross Reactivity: human, mouse, rat, monkey, bovine), ubiquitin (polyclonal, Z0458, Dako, 1:50, Species Cross Reactivity: human, mouse, rat), MAP2 (monoclonal, Chemicon, 1:400, Species Cross Reactivity: human, rat, mouse, bovine, chicken), Ki67 nuclear antigen (polyclonal, Novocastra - Leica Microsystems GmbH, Wetzlar, Germany; NCL-Ki67p, 1:1000, Species Cross Reactivity: human, mouse), PDGFR $\alpha$  (PDGFR $\alpha$ , polyclonal, #3164, Cell Signaling, 1:100, Species Cross Reactivity: human, mouse, rat).

After removal of the primary antibodies and repeated washes with PBS, cultures were incubated at room temperature (20 °C) for 45 min with secondary antibodies labeled with Alexa Fluor 594 or 488 (anti-mouse and/or anti rat, Molecular Probes - Life Technologies, Carlsbad, CA, USA). Samples were then colored with 4',6-diamidino-2-phenylindole dihydrochloride (DAPI; 0.3  $\mu$ g/ml, Roche Applied Science, Penzberg, Germany) for nuclear staining and rinsed with PBS for mounting and analysis. Microphotographs were taken using a Zeiss Axiovert 200 direct epifluorescence microscope (Axioptan 2; Carl Zeiss, Jena, Germany) or by confocal microscopy (Leica DM IRE2).

**Immunohistochemistry.** Mice (6 weeks, 8 and 11 months of age) were euthanized with Avertin (300 mg/kg) and transcardially perfused-fixed with 4% paraformaldehyde. Brains were post-fixed overnight, cryoprotected, frozen and

coronally sectioned (20  $\mu\text{m}$  thick) by cryostat. For the human specimen, sections (20  $\mu\text{m}$  thick) were obtained by cryostat, post-fixed with 4% paraformaldehyde and processed as murine samples. Sections were blocked with 10% normal goat serum and 1% Triton X-100 for 90 min and incubated overnight with the following primary antibodies: GFAP,  $\beta\text{tubIII}$ , MAP2, Lamp1, caspase3, ubiquitin, PDGFR $\alpha$  (see immunocytochemistry analysis for dilution), MBP (monoclonal, SMI 99P, Covance, 1:200, Species Cross Reactivity: mammalian), Dcx (C-18) (polyclonal, sc-8066, Santa Cruz Biotechnology, Dallas, TX, USA; 1:200, Species Cross Reactivity: mouse, rat). The fluorescent secondary antibodies used were labeled with Alexa Fluor 549 or 488 (Molecular Probes). DAPI (see immunocytochemistry analysis) was used as nuclear marker. Labeled samples were analyzed by fluorescence microscopy and by confocal microscopy (see immunocytochemistry analysis). Densitometric analysis of human specimen was performed by evaluation of confocal microscopy images ( $n=21$  cells, randomly chosen over  $n=7$  slices per sample) with Laser Pix Software (Bio-Rad Laboratories, Hercules, CA, USA).

**Image quantification and statistical analysis.** For immunocytochemistry, data are reported as percentages of labeled cells over the total number of nuclei  $\pm$  S.E.M. An average total amount of  $3 \times 10^3$  cells (identified by DAPI nuclear staining) was counted randomly from two coverslips per condition in each experiment. Each value represents the average of three independent experiments.

For immunohistochemistry, quantification of the percentage of GFAP + cells over total DAPI was performed in three regions of interest per section (cortex, sub-ventricular zone (each 200  $\mu\text{m}$  apart) spanning the central region of bregma 0 and adjacent striatum area, OBs). Each value represents the average of  $n=3$  animals unless differently stated in the text.

Statistical analysis was performed by *t*-test and two-ways ANOVA (Bonferroni test). Data are reported as mean  $\pm$  S.E.M. Data are considered not statistically significant unless indicated in the figures (\* indicates  $P \leq 0.05$ , \*\* indicates  $P \leq 0.01$ , \*\*\* indicates  $P \leq 0.001$ ).

**Western blot analysis.** Immunoblots were performed as described.<sup>33</sup> Polyvinylidene fluoride membranes (Millipore) were incubated with rat antibodies against IDS and Notch1 (100-401-407, Rockland) and monoclonal antibodies for glyceraldehyde 3-phosphate dehydrogenase (Sigma-Aldrich, St. Louis, MO, USA), the latter to normalize bands for equal loading of proteins per lane. Bands were quantified by densitometric analysis of the ECL-exposed films.

**Electron Microscopy analysis.** For standard EM, cell monolayers were washed with phosphate buffer 0.12M, fixed with 2% glutaraldehyde/4% paraformaldehyde in 0.12M phosphate buffer (30 min, 20 °C) and post-fixed with 2% OsO<sub>4</sub> in 0.1M sodium cacodylate buffer. After dehydration in ethanol and overnight infiltration (75% Epon-812, 25% ethanol), samples were embedded in Epon. Ultrathin sections (60 nm thickness) were doubly stained with uranyl acetate and lead citrate and examined with a Philips CM10microscope (Philips, Eindhoven, Netherlands). Electronic micrographs were captured with a slow scan CCD camera (S.I.S. Megaview III). Lysosomes were measured with Image J software 1.5.0\_10 (32 bit).

**IDS enzymatic assay.** IDS activity was measured by a fluorogenic assay<sup>34</sup> using the artificial substrate 4-methylumbelliferyl- $\alpha$ -L-iduronide-2-sulfate (MU- $\alpha$ -IdoA-2S; Moscerdam Substrates, Oegstgeest, Netherlands) according to the manufacturer's instructions. Enzyme activity was given as nmoles of substrate hydrolyzed in 4 h per mg of total protein or per ml of culture medium, using 4-methylumbelliferone (Sigma-Aldrich) as standard. Each value represents the average of three or four independent replicates.

## Conflict of Interest

The authors declare no conflict of interest.

**Acknowledgements.** We thank Anna Villa for densitometric analysis, Alessio Giavazzi, Daniela Ferrari and Manuel Fiorillo for precious support and collaboration. Human tissue was obtained from the NIHCD Brain and Tissue Bank for Developmental Disorders at the University of Maryland, Baltimore, MD, USA. The role of NIHCD Brain and Tissue Bank is to distribute tissue, and therefore, cannot endorse the studies performed or the interpretation of results. The project was funded by Fondazione Cellule Staminali di Terni and partly by the Brains for Brain Foundation (<http://www.brains4brain.eu>).

1. Muenzer J. Overview of the mucopolysaccharidoses. *Rheumatology (Oxford)* 2011; **50**: v4–v12.
2. Scarpa M, Almasy Z, Beck M, Bodamer O, Bruce IA, De Meirleir L *et al*. Mucopolysaccharidosis type II: European recommendations for the diagnosis and multidisciplinary management of a rare disease. *Orphanet J Rare Dis* 2011; **6**: 72.
3. Muenzer J, Beck M, Eng CM, Giugliani R, Harmatz P, Martin R *et al*. Long-term, open-labeled extension study of idursulfase in the treatment of Hunter syndrome. *Genet Med* 2011; **13**: 95–101.
4. Muenzer J, Beck M, Giugliani R, Suzuki Y, Tylki-Szymanska A, Valayannopoulos V *et al*. Idursulfase treatment of Hunter syndrome in children younger than 6 years: results from the Hunter Outcome Survey. *Genet Med* 2011; **13**: 102–109.
5. Muenzer J, Bodamer O, Burton B, Clarke L, Frenking GS, Giugliani R *et al*. The role of enzyme replacement therapy in severe Hunter syndrome—an expert panel consensus. *Eur J Pediatr* 2012; **171**: 181–188.
6. Higuchi T, Shimizu H, Fukuda T, Kawagoe S, Matsumoto J, Shimada Y *et al*. Enzyme replacement therapy (ERT) procedure for mucopolysaccharidosis type II (MPS II) by intraventricular administration (IVA) in murine MPS II. *Mol Genet Metab* 2012; **107**: 122–128.
7. Politto VA, Abbondante S, Polishchuk RS, Nusco E, Salvia R, Cosma MP. Correction of CNS defects in the MPSII mouse model via systemic enzyme replacement therapy. *Hum Mol Genet* 2010; **19**: 4871–4885.
8. Cardone M, Politto VA, Pepe S, Mann L, D'Azzo A, Auricchio A *et al*. Correction of Hunter syndrome in the MPSII mouse model by AAV2/8-mediated gene delivery. *Hum Mol Genet* 2006; **15**: 1225–1236.
9. Vogler C, Levy B, Grubb JH, Galvin N, Tan Y, Kakkis E *et al*. Overcoming the blood-brain barrier with high-dose enzyme replacement therapy in murine mucopolysaccharidosis VII. *Proc Natl Acad Sci USA* 2005; **102**: 14777–14782.
10. Muenzer J, Gucavas-Calikoglu M, McCandless SE, Schuetz TJ, Kimura A. A phase I/II clinical trial of enzyme replacement therapy in mucopolysaccharidosis II (Hunter syndrome). *Mol Genet Metab* 2007; **90**: 329–337.
11. Muenzer J, Wraith JE, Beck M, Giugliani R, Harmatz P, Eng CM *et al*. A phase II/III clinical study of enzyme replacement therapy with idursulfase in mucopolysaccharidosis II (Hunter syndrome). *Genet Med* 2006; **8**: 465–473.
12. Wraith JE. Enzyme replacement therapy with idursulfase in patients with mucopolysaccharidosis type II. *Acta Paediatr Suppl* 2008; **97**: 76–78.
13. Tomanin R, Zanetti A, Zaccariotto E, D'Avanzo F, Belletato CM, Scarpa M. Gene therapy approaches for lysosomal storage disorders, a good model for the treatment of mendelian diseases. *Acta Paediatr* 2012; **101**: 692–701.
14. Givogri MI, Bottai D, Zhu HL, Fasano S, Lamorte G, Brambilla R *et al*. Multipotential neural precursors transplanted into the metachromatic leukodystrophy brain fail to generate oligodendrocytes but contribute to limit brain dysfunction. *Dev Neurosci* 2008; **30**: 340–357.
15. Lemonnier T, Blanchard S, Toli D, Roy E, Bigou S, Froissart R *et al*. Modeling neuronal defects associated with a lysosomal disorder using patient-derived induced pluripotent stem cells. *Hum Mol Genet* 2011; **20**: 3653–3666.
16. Marshall GP 2nd, Reynolds BA, Laywell ED. Using the neurosphere assay to quantify neural stem cells *in vivo*. *Curr Pharm Biotechnol* 2007; **8**: 141–145.
17. Reynolds BA, Rietze RL. Neural stem cells and neurospheres—re-evaluating the relationship. *Nat Methods* 2005; **2**: 333–336.
18. Heuer GG, Skorupa AF, Prasad Alur RK, Jiang K, Wolfe JH. Accumulation of abnormal amounts of glycosaminoglycans in murine mucopolysaccharidosis type VII neural progenitor cells does not alter the growth rate or efficiency of differentiation into neurons. *Mol Cell Neurosci* 2001; **17**: 167–178.
19. Ravikumar B, Sarkar S, Davies JE, Futter M, Garcia-Arencibia M, Green-Thompson ZW *et al*. Regulation of mammalian autophagy in physiology and pathophysiology. *Physiol Rev* 2010; **90**: 1383–1435.
20. Politto VA, Cosma MP. IDS crossing of the blood-brain barrier corrects CNS defects in MPSII mice. *Am J Hum Genet* 2009; **85**: 296–301.
21. Jackson EL, Garcia-Verdugo JM, Gil-Perotin S, Roy M, Quinones-Hinojosa A, VandenBerg S *et al*. PDGFR alpha-positive B cells are neural stem cells in the adult SVZ that form glioma-like growths in response to increased PDGF signaling. *Neuron* 2006; **51**: 187–199.
22. Vitner EB, Platt FM, Futerman AH. Common and uncommon pathogenic cascades in lysosomal storage diseases. *J Biol Chem* 2010; **285**: 20423–20427.
23. Ballabio A, Gieselmann V. Lysosomal disorders: from storage to cellular damage. *Biochim Biophys Acta* 2009; **1793**: 684–696.
24. Decker L, ffrench-Constant C. Lipid rafts and integrin activation regulate oligodendrocyte survival. *J Neurosci* 2004; **24**: 3816–3825.
25. Kazanis I, Lathia JD, Vadakkan TJ, Raborn E, Wan R, Mughal MR *et al*. Quiescence and activation of stem and precursor cell populations in the subependymal zone of the mammalian brain are associated with distinct cellular and extracellular matrix signals. *J Neurosci* 2010; **30**: 9771–9781.
26. Chojnacki A, Mak G, Weiss S. PDGFRalpha expression distinguishes GFAP-expressing neural stem cells from PDGF-responsive neural precursors in the adult periventricular area. *J Neurosci* 2011; **31**: 9503–9512.
27. Fager G, Camejo G, Olsson U, Ostergren-Lunden G, Lustig F, Bondjers G. Binding of platelet-derived growth factor and low density lipoproteins to glycosaminoglycan

- species produced by human arterial smooth muscle cells. *J Cell Physiol* 1995; **163**: 380–392.
28. Garcia-Olivas R, Hoebeke J, Castel S, Reina M, Fager G, Lustig F *et al*. Differential binding of platelet-derived growth factor isoforms to glycosaminoglycans. *Histochem Cell Biol* 2003; **120**: 371–382.
29. Meng XL, Shen JS, Kawagoe S, Ohashi T, Brady RO, Eto Y. Induced pluripotent stem cells derived from mouse models of lysosomal storage disorders. *Proc Natl Acad Sci USA* 2010; **107**: 7886–7891.
30. Woodruff RH, Fruttiger M, Richardson WD, Franklin RJ. Platelet-derived growth factor regulates oligodendrocyte progenitor numbers in adult CNS and their response following CNS demyelination. *Mol Cell Neurosci* 2004; **25**: 252–262.
31. Vescovi AL, Reynolds BA, Fraser DD, Weiss S. bFGF regulates the proliferative fate of unipotent (neuronal) and bipotent (neuronal/astroglial) EGF-generated CNS progenitor cells. *Neuron* 1993; **11**: 951–966.
32. Gritti A, Frolichsthal-Schoeller P, Galli R, Parati EA, Cova L, Pagano SF *et al*. Epidermal and fibroblast growth factors behave as mitogenic regulators for a single multipotent stem cell-like population from the subventricular region of the adult mouse forebrain. *J Neurosci* 1999; **19**: 3287–3297.
33. Carlessi L, De Filippis L, Lecis D, Vescovi A, Delia D. DNA-damage response, survival and differentiation in vitro of a human neural stem cell line in relation to ATM expression. *Cell Death Differ* 2009; **16**: 795–806.
34. Voznyi YV, Keulemans JL, van Diggelen OP. A fluorimetric enzyme assay for the diagnosis of MPS II (Hunter disease). *J Inherit Metab Dis* 2001; **24**: 675–680.



**Cell Death and Disease** is an open-access journal published by **Nature Publishing Group**. This work is licensed under a **Creative Commons Attribution-NonCommercial-NoDerivs 3.0 Unported License**. To view a copy of this license, visit <http://creativecommons.org/licenses/by-nc-nd/3.0/>

Supplementary Information accompanies this paper on Cell Death and Disease website (<http://www.nature.com/cddis>)